中国激光

基于梅斯林对切光子筛的相位型液晶空间光调制器的干涉校准

王港伟[1,2]，周梦宇[1,3]，张军勇[1,4*]，刘诚[1**]

[1]中国科学院上海光学精密机械研究所高功率激光物理联合实验室，上海 201800；
[2]中国科学院大学，北京 100049；
[3]上海科技大学物质科学与技术学院，上海 201210；
[4]上海交通大学IFSA合作创新中心，上海 200240

摘要 基于梅斯林对切光子筛，提出了一个小程差的干涉测量方案以校准空间光调制器。该方案不仅提供了参考坐标系，补偿了系统振动对定标结果的扰动，而且获得了高信噪比的干涉光斑，降低了测量系统对探测器灵敏度的要求。在批量提取干涉光斑质心后，通过参考坐标系转换，得到了相位调制曲线。该曲线通过了波前分析仪的相位检定，632.8 nm 和 488 nm 波长光的标定曲线的残差最大峰谷值小于 0.012λ（λ为波长）。结果表明，该方案是一个适用于空间光调制器的高稳定高精度的干涉校准方法。

关键词 测量；空间光调制器；相位校准；衍射光学元件；干涉

中图分类号 O436 **文献标志码** A **DOI**：10.3788/CJL230758

1 引 言

液晶空间光调制器（SLM）是一种可以对光的相位信息进行定量调控的数字器件，被应用于自适应光学[1-3]、全息三维显示[4-6]、波前传感[7-8]、光束整形[9-12]等诸多领域。在理想情况下，SLM 中加载的灰度和位移的对应关系与 SLM 手册里的查找表（LUT）是相同的，但是调制面板每层材料对环境变化的响应不同，且液晶对调制电压有非线性响应，受这些潜在因素的影响，实际使用 SLM 进行相位调制时存在着调制误差。同时，由于 SLM 的相位调制是通过改变 e 光的等效折射率来实现的，当不同波长光入射时，液晶材料的双折射效应会有所变化。因此当 SLM 的实际工作波长与预设波长不同时，为了获得准确的相位调制，须重新对 SLM 进行标定[13]。除衍射法外，一般利用干涉条纹的位移来表征相位调制的结果，常用方法包括双缝干涉测量法[14]、迈克耳孙干涉法[15-16]、马赫-曾德尔干涉法[17]和 Twyman-Green 干涉法[18]等。其中，双缝干涉单次测量只能表征一条缝上的相位变化，不能表征整个器件的调制特性，同时还要重新设置光路、更换器件。采集干涉条纹图像时系统很难保持稳定，不可避免地受到环境的扰动，导致定标结果出现一定的误差。迈克耳孙干涉法、马赫-曾德尔干涉法和 Twyman-Green 干涉法采用双光路，对测量光路的稳定性要求更高。为了解决环境造成的条纹位移误差问题，文献[19]提出了一种利用背景光构造绝对参考系的定标方法，但是干涉条纹与艾里斑的重合导致条纹对比度不理想，且该方法对探测器灵敏度的要求较高，具有较大的局限性。

为了在满足绝对参考系条件、减小振动误差的条件下获取较为理想的干涉条纹，本文提出了一种基于梅斯林对切光子筛的干涉校准方法。基于梅斯林干涉装置，加工具有不同焦距的对切光子筛，其中一个光子筛是固定的，另一个光子筛对应的 SLM 灰度在 0～255 范围内线性变化。将经过参考光子筛的背景光产生的艾里斑作为绝对坐标系的原点。由于两个光子筛的焦距差是小程差，两焦点中间位置处的干涉条纹具有高信噪比，通过质心坐标获取了条纹位移量。最后使用波前传感器对 SLM 相位进行量化处理，其结果与梅斯林干涉校准 SLM 的相位曲线基本吻合，有效证明了所提方法的有效性和准确性。

收稿日期：2023-04-24；**修回日期**：2023-05-23；**录用日期**：2023-06-15；**网络首发日期**：2023-07-04

基金项目：国家自然科学基金（62175245，62105345）、上海市青年科技英才扬帆计划（21YF1453700）、中国科学院战略性先导科技专项（A 类）（XDA25020302）

通信作者：*zhangjy829@siom.ac.cn；**chengliu@siom.ac.cn

2 方法与理论基础

传统的梅斯林干涉装置[20]如图 1(a)所示，将一块凸透镜沿表面直径剖为两部分(L_1和L_2)，并在光轴方向错开一段距离，在相同焦距、不同物距下可获得轴上两相干点光源S_1和S_2，在两个光源的叠加区S_1MS_2内会出现干涉现象。这种干涉装置和杨氏双孔、洛埃镜、双面镜、双棱镜、Billet对切透镜等装置相似，是一种双光束分波前形式的干涉装置。梅斯林干涉还有另一种实现方法[21]，如图 1(b)所示，用两块焦距分别为f_1和f_2的凸薄透镜L_1'和L_2'，将它们沿表面直径剖开，各取一半构成一块共轴横向组合透镜L，在轴上有两个实像点S_1'、S_2'。这种方式所获得的干涉条纹和传统梅斯林干涉装置得到的条纹相同，只是干涉级次有些差异。

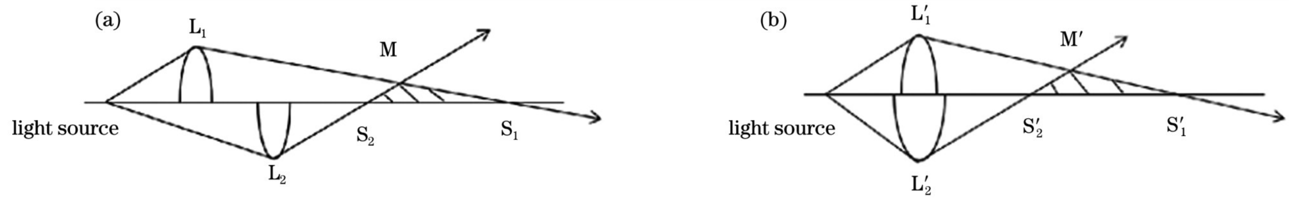

图 1 梅斯林干涉结构。(a)不同物距；(b)不同焦距

Fig. 1 Meslin interference structures. (a) Different object distance; (b) different focal length

相对于基于折射透镜的梅斯林对切结构，基于衍射透镜的梅斯林对切结构更容易设计与加工。光子筛作为一类典型的衍射透镜，是由Kipp等[22]提出的。菲涅耳波带片的通光环被大量随机的圆孔代替，圆孔直径等于所在环宽的1.53倍，此时获得的焦斑直径小于对应数值孔径的菲涅耳波带片产生的焦斑，同时光子筛能够很好地抑制焦斑的旁瓣。对于在光学段使用的光子筛，其制备方法如下：一般在石英基底上镀铬，通过光刻工艺获得通光和不通光的若干圆孔，圆孔沿菲涅耳波带片的通光环排布。在标量衍射条件下，小孔尺寸通常为波长的数倍，而几个微米直径的圆孔对于纳米精度的光刻工艺来说，可以认为是理想的圆孔图案。基于图 1(b)所示的梅斯林结构的对切光子筛的实物如图 2 所示，其焦距分别为 240 mm 和 242.4 mm，图中所示为光子筛的中心局部区域。当探测器位于两焦点的重叠区域时，出现干涉条纹。当保持一个光子筛对应的 SLM 灰度不变时，另一个光子筛对应的 SLM 灰度在 0~255 之间线性变化，在探测器靶面上可以观察到干涉光斑的移动。将参考光子筛产生的光斑作为绝对坐标系的原点，由于梅斯林对切光子筛与参考光子筛的位置在制作时便已固定，通过计算干涉光斑相对绝对坐标系原点的距离变化，可以消除光路的振动影响，得到光斑的真实位移量。仿真结果如图 3 所示。当 SLM 灰度发生变化时，干涉光斑会发生移动，其位移量对应的相位值为

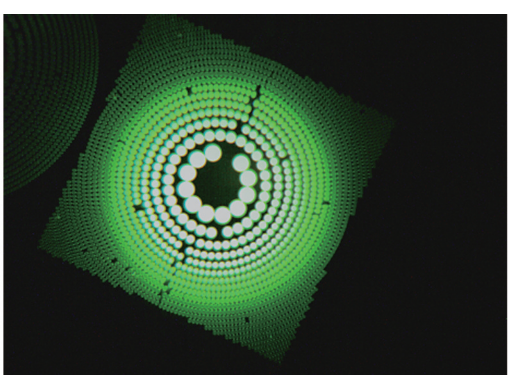

图 2 梅斯林对切光子筛的显微镜图

Fig. 2 Micrograph of Meslin-split photon sieves

$$\varphi = 2\pi a/d, \tag{1}$$

式中：a为干涉光斑的移动量；d为干涉光斑周期。

由图 3 所示的相移-干涉条纹移动距离曲线图可以看出，干涉条纹的移动距离与相位延迟之间存在线性关系。SLM 不同的灰度对应不同的相位调制量，在得到干涉条纹位移后，通过式(1)能够直接求解出对应灰度下的相移量。

3 实验与讨论

3.1 标定实验

为了证明上述基于梅斯林对切光子筛的干涉校准方法有效可行，本文开展了共光路实验，实验光路如图 4 所示。以光纤激光器作为光源，激光经扩束器扩束后，被分束器(BS)分为两路，其中一路光经过起偏器后到达 SLM(分辨率为 1920×1080，像元尺寸为 6.4 μm)，获得加载灰度值后反射回光路，再次经过分束器并穿过梅斯林对切光子筛，最终由探测器(分辨率为 3856×2764，像元尺寸为 1.67 μm)记录干涉光斑图像。保持灰度值不变的光子筛的焦距为 240 mm，加载 0~255 灰度值的光子筛的焦距为 242.4 mm。当灰度变化时，所有干涉光斑将同步移动；由于参考光子筛用于产生绝对坐标系的原点，故很容易确定干涉光斑的位移量。实验结果如图 5 所示，图 5(b)为图 5(a)的局部放大，共拍摄 32 幅，等距取样显示 16 幅。通过质心算法可以得到条纹的周期为 30 μm，与理论分析结果是一致的。

对多次实验得到的图像进行批量处理，得到干涉光斑质心与绝对坐标系原点的位置。在同一帧干涉

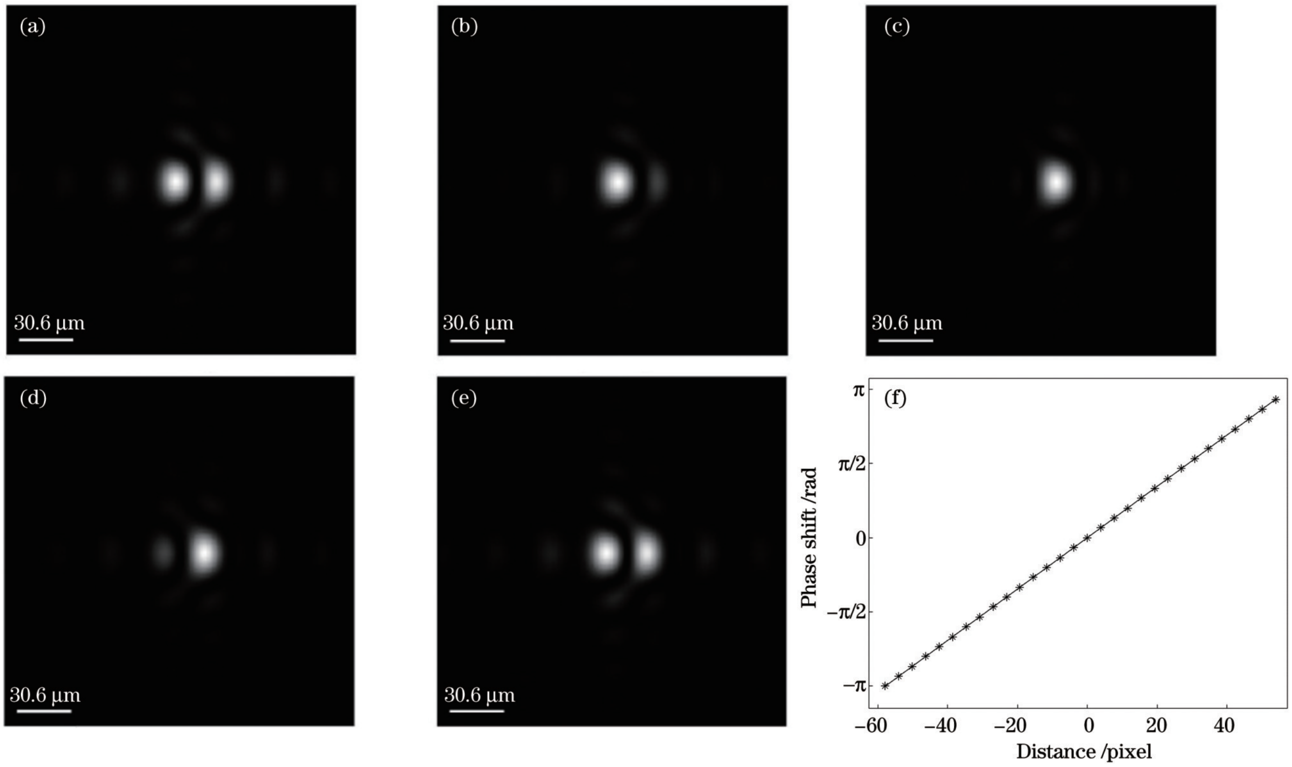

图3　仿真结果及相移-干涉条纹移动距离曲线。(a)相位延迟为 $-\pi$；(b)相位延迟为 $-\pi/2$；(c)相位延迟为0；(d)相位延迟为 $\pi/2$；(e)相位延迟为 π；(f)相移-干涉条纹移动距离曲线

Fig. 3　Simulation results and phase shift versus moving distance of interference fringe. (a) Phase shift of $-\pi$; (b) phase shift of $-\pi/2$; (c) phase shift of 0; (d) phase shift of $\pi/2$; (e) phase shift of π; (f) phase shift versus moving distance of interference fringe

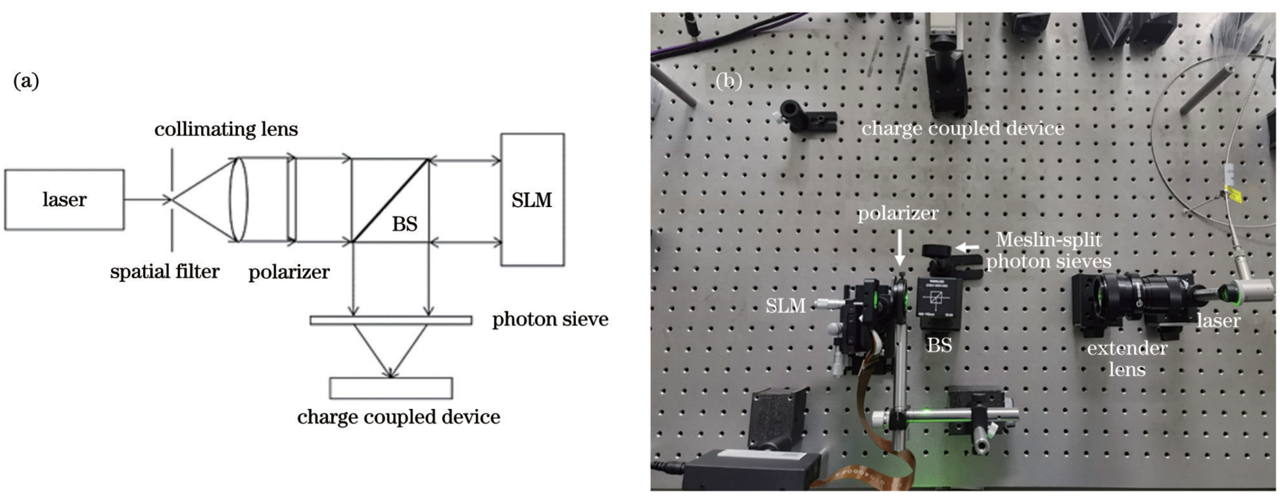

图4　梅斯林对切光子筛标定相位曲线的实验光路。(a)原理图；(b)光路图

Fig.4　Experimental optical path for phase calibration with Meslin-split photon sieves. (a) Schematic; (b) optical path diagram

光斑图中，绝对坐标系原点的偏移是由系统振动引起的，但干涉光斑与绝对坐标系原点的相对位置不变，其差值可用来补偿系统振动。随着灰度的改变，干涉光斑向一侧移动。利用干涉光斑质心的偏移量，计算获得与灰度对应的相位值，通过数据拟合得到灰度-相位曲线，其拟合函数为 $y=-0.003994x+0.9868$，方差为0.9967（该值越接近常数1，表示拟合性越好），均方根误差为0.0174，如图6所示，其中 λ 为波长。

当氦氖激光器更换成波长为488 nm的激光器时，重复上述过程可以得到32幅干涉图，其中灰度值为136的干涉光斑图如图7(a)所示，处理得到的灰度-相位曲线如图7(b)所示。其拟合函数为 $y=-0.005839x+1.424$，方差为0.9972，均方根误差为0.0234。

3.2　波前传感器检定SLM的校准精度

为了检定SLM相位校准的精度，将梅斯林对切光子筛替换成波前传感器进行相位检定，测量光路

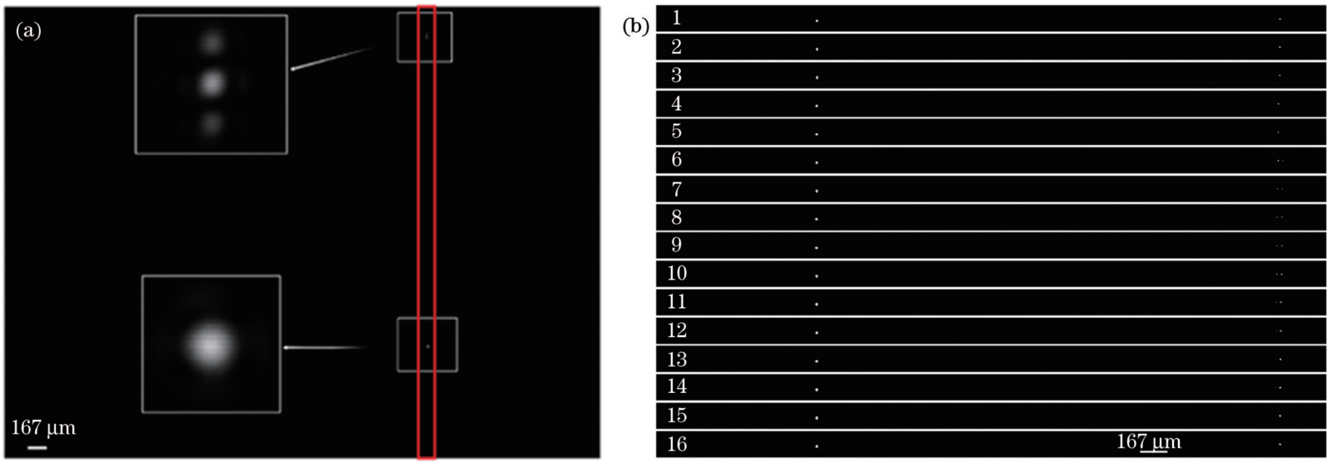

图 5　633 nm 激光下的 SLM 相位标定实验数据。(a)干涉光斑;(b)图 5(a)的局部放大

Fig. 5　Experimental data of SLM phase calibration under 633 nm laser. (a) Interference spots; (b) local magnification of Fig. 5(a)

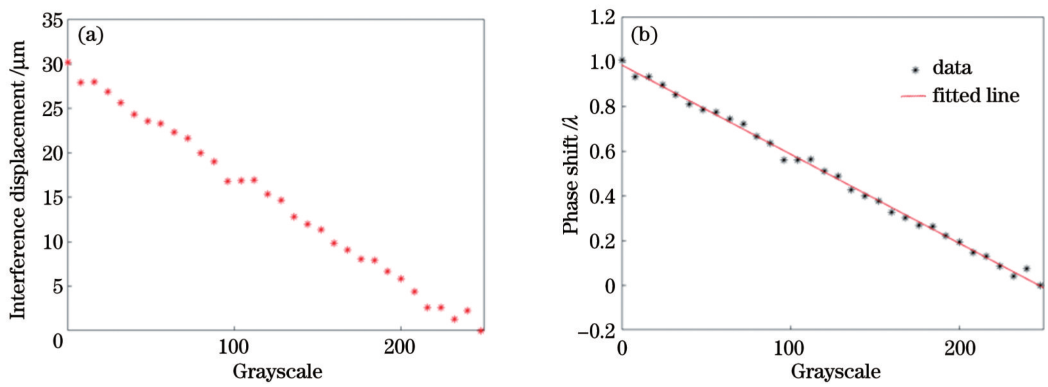

图 6　633 nm 激光下的 SLM 相位标定实验结果。(a)灰度与干涉位移的关系;(b)灰度与相移的关系

Fig. 6　Experimental results of SLM phase calibration under 633 nm laser. (a) Grayscale versus interference displacement; (b) grayscale versus phase shift

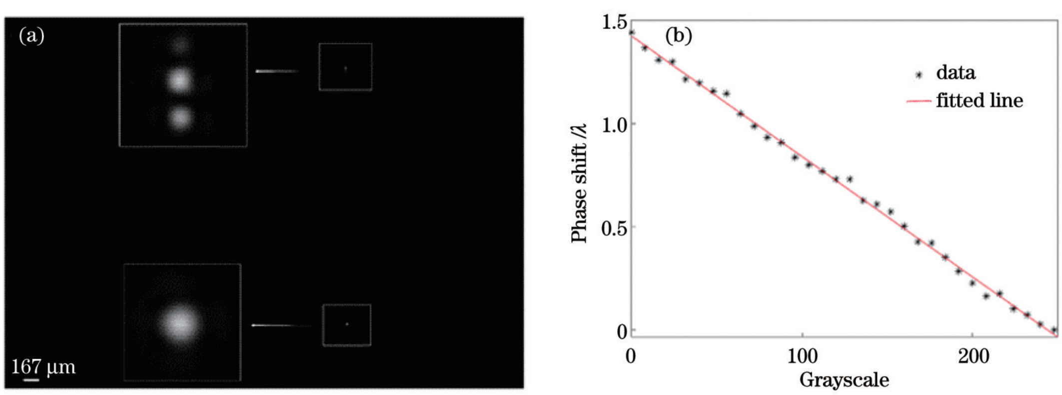

图 7　488 nm 激光下的 SLM 相位标定实验结果。(a)干涉光斑;(b)灰度与相移的关系

Fig. 7　Experimental results of SLM phase calibration under 488 nm laser. (a) Interference spots; (b) grayscale versus phase shift

如图 8 所示。以氦氖激光对 SLM 的相位校准为例，在 SLM 上加载超高斯灰度图，平顶部分为测试对象，函数表达式为

$$f(r)=\exp(-0.5\times r^{2n}/\omega^{2n}),\tag{2}$$

式中：极径 r=0～1.8 mm；束腰宽度 ω=1.2 mm；超高斯光束的阶数 n=4。

图 9 给出了 SLM 灰度值为 34、114、178 和 226 时对应的相移量，分别为 0.8444λ、0.5320λ、0.2701λ 和

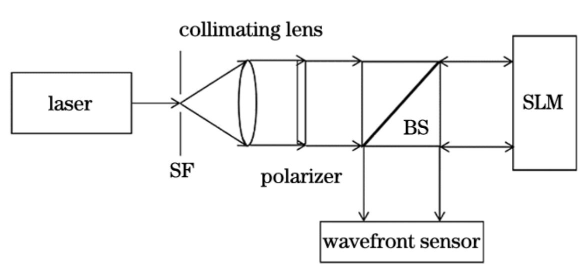

图 8　波前传感器实验光路

Fig. 8　Experimental optical path of wavefront sensor

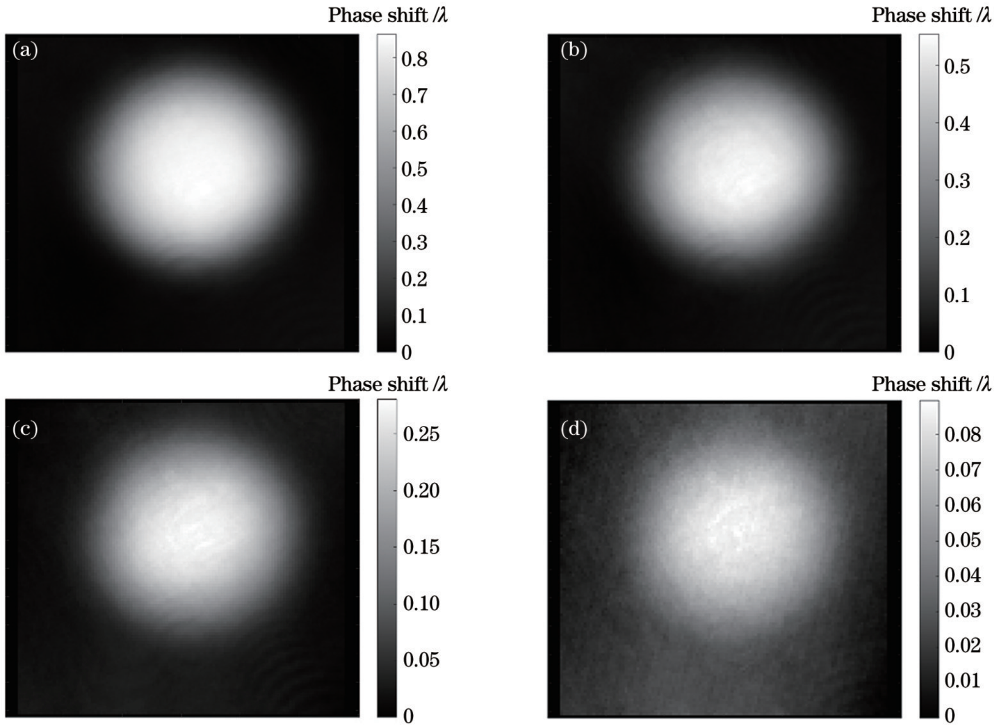

图 9 633 nm激光入射下不同灰度值SLM对应的相移。(a)灰度值为34;(b)灰度值为114;(c)灰度值为178;(d)灰度值为226

Fig. 9 Phase shifts corresponding to SLMs with different grayscale values under 633 nm laser incidence. (a) Grayscale value of 34; (b) grayscale value of 114; (c) grayscale value of 178; (d) grayscale value of 226

0.0813λ(选取光强均匀位置,划定区域,计算加权平均值得到)。而氦氖激光SLM校准的灰度-相位曲线所对应的值依次为0.8510λ、0.5315λ、0.2759λ和0.0842λ。定标残差的最大峰谷值为0.0066λ,均方根误差为0.0046。

同样对于488 nm的激光入射,图10给出了SLM灰度值为129、177、193、225时对应的相移量,分别为0.6797λ、0.3978λ、0.2854λ和0.1037λ。而波长为488 nm

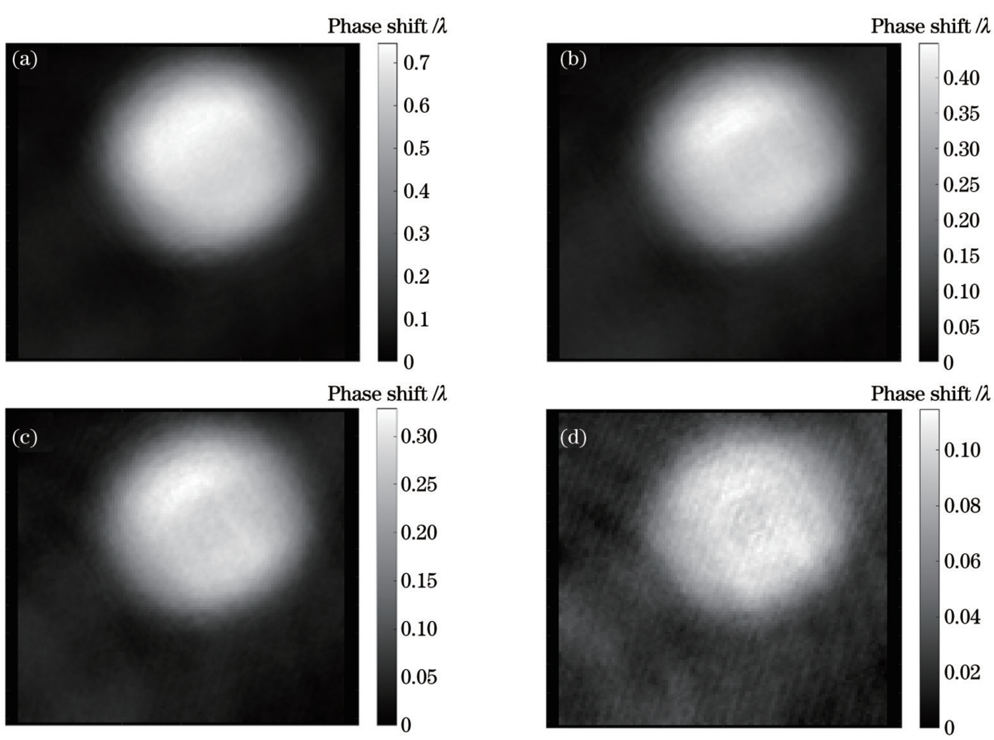

图 10 488 nm激光入射下不同灰度值SLM对应的相移。(a)灰度值为129;(b)灰度值为177;(c)灰度值为193;(d)灰度值为225

Fig. 10 Phase shifts corresponding to SLMs with different grayscale values under 488 nm laser incidence. (a) Grayscale value of 129; (b) grayscale value of 177; (c) grayscale value of 193; (d) grayscale value of 225

的 SLM 校准的灰度-相位曲线所对应的值依次为 0.6708λ、0.3905λ、0.2971λ 和 0.1102λ。定标残差的最大峰谷值为 0.0117λ，均方根误差为 0.0088。

图 11 给出了不同波长光入射下波前传感器检定的灰度-相位曲线图，可以看出，当两个波长光分别入射 SLM 时，梅斯林对切光子筛定标的结果与波前传感器高度吻合，定标曲线的残差最大峰谷值优于 0.012λ。由此可见，上述 SLM 定标的方法有效可行，且具有足够的精度，这为 SLM 的高精度应用提供了保障。

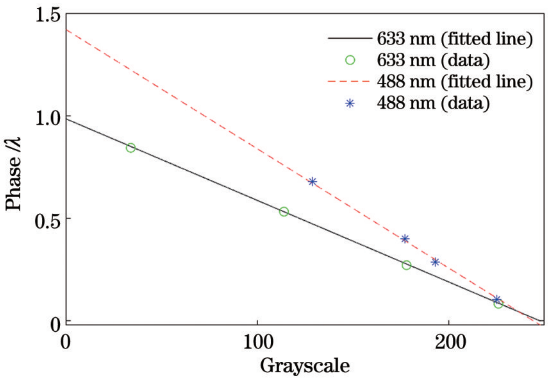

图 11 不同波长光入射下波前传感器检定的灰度-相位曲线图

Fig. 11 Grayscale-phase curves verified by wavefront sensor under different wavelength incident light

4 结 论

提出了一种基于梅斯林对切光子筛的干涉校准方法。梅斯林对切光子筛在焦点中间位置形成具有高信噪比的干涉光斑，同时又将干涉光斑与绝对坐标系原点分离开，从而使该校准方案对光路稳定性和探测器灵敏度要求不高，满足了不同环境下的 SLM 校准需求。利用波前传感器检定了 SLM 校准的灰度-相位曲线，证明了梅斯林对切光子筛对 SLM 的干涉校准具有高精度和高稳定性，能够满足不同 SLM 应用精度需求。

致谢 感谢杜彤耀提供了用于相位检定的波前传感器设备，李优协助完成了实验，以及张秀平在本文写作过程中给出了建议！

参 考 文 献

[1] Psaltis D, Brady D, Wagner K. Adaptive optical networks using photorefractive crystals[J]. Applied Optics, 1988, 27(9): 1752-1759.

[2] Li C, Xia M L, Mu Q Q, et al. High-precision open-loop adaptive optics system based on LC-SLM[J]. Optics Express, 2009, 17(13): 10774-10781.

[3] Shen X L, Kahn J M, Horowitz M A. Compensation for multimode fiber dispersion by adaptive optics[J]. Optics Letters, 2005, 30(22): 2985-2987.

[4] Ma Q G, Cao L C, He Z H, et al. Progress of three-dimensional light-field display[J]. Chinese Optics Letters, 2019, 17(11): 111001.

[5] Hasegawa S, Hayasaki Y, Nishida N. Holographic femtosecond laser processing with multiplexed phase Fresnel lenses[J]. Optics Letters, 2006, 31(11): 1705-1707.

[6] Finke G, Kujawińska M, Kozacki T. Visual perception in multi SLM holographic displays[J]. Applied Optics, 2015, 54(12): 3560-3568.

[7] Murphy K, Burke D, Devaney N, et al. Experimental detection of optical vortices with a Shack-Hartmann wavefront sensor[J]. Optics Express, 2010, 18(15): 15448-15460.

[8] Wang B Y, Han L, Yang Y, et al. Wavefront sensing based on a spatial light modulator and incremental binary random sampling[J]. Optics Letters, 2017, 42(3): 603-606.

[9] Hu L F, Xuan L, Liu Y J, et al. Phase-only liquid crystal spatial light modulator for wavefront correction with high precision[J]. Optics Express, 2004, 12(26): 6403-6409.

[10] Chen Z Z, Zeng T T, Qian B J, et al. Complete shaping of optical vector beams[J]. Optics Express, 2015, 23(14): 17701-17710.

[11] Burger L, Litvin I, Ngcobo S, et al. Implementation of a spatial light modulator for intracavity beam shaping[J]. Journal of Optics, 2015, 17(1): 015604.

[12] Huang D J, Fan W, Cheng H, et al. Wavefront control of laser beam using optically addressed liquid crystal modulator[J]. High Power Laser Science and Engineering, 2018, 6(2): e20.

[13] 刘冬梅，刘娟，张昭，等. 相位型液晶空间光调制器初始相位的校准与多波长响应的研究[J]. 激光与光电子学进展，2012, 49(4): 041203.
Liu D M, Liu J, Zhang Z, et al. Study of initial phase calibration and multi-wavelength response of phase-only spatial light modulator[J]. Laser & Optoelectronics Progress, 2012, 49(4): 041203.

[14] 陈怀新，隋展，陈祯培，等. 液晶电视 LCTV 的光学调制特性及其应用[J]. 中国激光，2000, 27(8): 741-745.
Chen H X, Sui Z, Chen Z P, et al. Optical modulation characteristics of liquid crystal television (LCTV) and its application in optics information processing[J]. Chinese Journal of Lasers, 2000, 27(8): 741-745.

[15] 葛爱明，隋展，徐克璹. 反射型 LCOS 器件纯相位调制特性的研究[J]. 物理学报，2003, 52(10): 2481-2485.
Ge A M, Sui Z, Xu K S. Characteristics of phase-only modulation using a reflective liquid crystal on silicon device[J]. Acta Physica Sinica, 2003, 52(10): 2481-2485.

[16] Kelly T L, Munch J. Phase-aberration correction with dual liquid-crystal spatial light modulators[J]. Applied Optics, 1998, 37(22): 5184-5189.

[17] Reichelt S. Spatially resolved phase-response calibration of liquid-crystal-based spatial light modulators[J]. Applied Optics, 2013, 52(12): 2610-2618.

[18] Zhang H X, Zhang J A, Wu L Y. Evaluation of phase-only liquid crystal spatial light modulator for phase modulation performance using a Twyman-Green interferometer[J]. Measurement Science and Technology, 2007, 18(6): 1724-1728.

[19] Li Y, Li Y C, Zhang J Y, et al. Generalized phase calibration method of liquid crystal spatial light modulator with absolute reference system of obnoxious background light[J]. Optics and Lasers in Engineering, 2020, 132: 106132.

[20] 冯才鑫，孟庆国，冯立峰，等. 单色点光源经梅斯林透镜的干涉现象分析[J]. 物理与工程，2019, 29(5): 68-71, 77.
Feng C X, Meng Q G, Feng L F, et al. Analysis of interference phenomenon for Messlin lens[J]. Physics and Engineering, 2019, 29(5): 68-71, 77.

[21] 潘维济，李婉茹. 梅斯林干涉条纹[J]. 大学物理，1985, 4(9): 31-33.
Pan W J, Li W R. Myslin interference fringe[J]. College Physics, 1985, 4(9): 31-33.

[22] Kipp L, Skibowski M, Johnson R L, et al. Sharper images by focusing soft X-rays with photon sieves[J]. Nature, 2001, 414(6860): 184-188.

Interferometric Calibration of Phase-Only Liquid Crystal Spatial Light Modulators Based on Meslin-Split Photon Sieves

Wang Gangwei[1,2], Zhou Mengyu[1,3], Zhang Junyong[1,4*], Liu Cheng[1**]

[1]National Laboratory on High Power Laser and Physics, Shanghai Institute of Optics and Fine Mechanics, Chinese Academy of Sciences, Shanghai 201800, China;

[2]University of Chinese Academy of Sciences, Beijing 100049, China;

[3]School of Physical Science and Technology, ShanghaiTech University, Shanghai 201210, China;

[4]Collaborative Innovation Center of IFSA, Shanghai Jiao Tong University, Shanghai 200240, China

Abstract

Objective A spatial light modulator (SLM) is a digital device that quantitatively modulates light phase information. Ideally, the phase shift is linearly proportional to the grayscale, which is loaded into the SLM. However, the SLM grayscale is not linear with respect to the modulation voltage. In addition, when the incident wavelength is inconsistent with the working wavelength, the phase shift changes under the same grayscale. Therefore, the SLM must be calibrated before use. The traditional phase calibration of SLM is mainly realized through double-slit interference fringes, where the phase shift depends on the shift in the interference fringes. Unfortunately, owing to environmental vibrations, traditional phase calibration methods do not have adequate precision. To improve the measurement precision of the SLM phase calibration, even with environmental vibration, a self-reference interference method with Meslin-split photon sieves is proposed to compensate for system perturbation.

Methods Meslin-split photon sieves with two different focal lengths are fabricated on the same chrome. The optical detector is located in the middle of the two focal planes, and it records the interference fringes. In the experiment, a laser is used as the light source, which is collimated and expanded after a deflector, and divided into two paths using a beam splitter. One light beam reaches the SLM, where it is loaded with grayscale and reflected back to the beam splitter, and then passes through the Mesin-split photon sieves. However, owing to the influence of system jitter and other factors in the experiment, the interference spot results in a displacement error. The absolute coordinate origin of the measurement system is introduced to improve the measurement accuracy and robustness of the optical system. After a simple calculation, the absolute displacement is converted into the displacement relative to the absolute coordinate origin, which effectively reduces the environmental perturbation. The corresponding interference fringes are recorded when the greyscale maps are sequentially loaded into the SLM. In this case, the shift distance between the interference fringe and the absolute coordinate origin is calculated, and the modulated phase shifts corresponding to different grayscale values are calculated. The phase shift as a function of the grayscale is obtained by fitting the measured greyscale to the phase relationship.

Results and Discussions A common optical-path experimental scheme is used to calibrate the laser at 633 nm and 488 nm. Taking 633 nm laser illumination as an example, the grayscale is changed from 0 to 255, and the sampling interval is set 8. Thus, 32 frames of interference fringes are sequentially recorded. First, the absolute coordinate origin is calculated using the weighted centroid algorithm. The center coordinates of the interference fringes are calculated in the same manner. The center coordinates of the interference fringes are used to subtract the absolute coordinate origin and the shift of the interference fringes is obtained. The difference above is denoted by the baseline corresponding to the grayscale of zero. The differences corresponding to other grayscales are used to subtract the baseline, the absolute shifts of the interference fringes are successively obtained, and the environmental perturbation is completely eliminated. Finally, a grayscale-phase curve is obtained by linear fitting. The operation on the 488 nm laser illumination is the same as that on the 633 nm laser illumination. The variances of the fitted functions are 0.9967 and 0.9972 for the two wavelengths, respectively. As evidenced by the data, the closer the value is to 1, the better the obtained results. To verify the accuracy of the phase calibration of the SLM performed by the Meslin-split photon sieves, the Mesin-split photon sieves and charge coupled device are replaced by the wavefront sensor for phase measurement. For convenience, a super-Gaussian beam is used for the phase measurement. The experimental results show that the phase values of wavefront sensor agree well with the grayscale phase values obtained using our proposed self-reference interferometric method with Meslin-split photon sieves. The experimental results verify that the phase calibration of the SLM with Meslin-split photon sieves has high accuracy and good robustness.

Conclusions This study presents a self-reference interferometric calibration method using Meslin-split photon sieves that is robust and easy to operate. The Meslin-split photon sieves form interferometric frings with a high signal-to-noise ratio in the middle of the two focal planes, while the absolute coordinate origin is generated by another independent photon sieve to make the calibration scheme less demanding in terms of optical path stability and detector sensitivity, as well as meet the requirements of SLM calibration in different environments. The grayscale-phase curve of the SLM calibration is verified by the wavefront sensor, which demonstrates that the photon sieves have high accuracy and stability for SLM interferometric calibration and are capable of meeting the accuracy requirements of different SLM applications.

Key words measurement; spatial light modulator; phase calibration; diffraction optical elements; interference